# $\beta$ decay of $^{47}$Ar

L. Weissman,[1,*] O. Arnd,[2] U. Bergmann,[3] A. Brown,[1] R. Catherall,[3] J. Cederkall,[3] I. Dillmann,[2] O. Hallmann,[2] L. Fraile,[3,4] S. Franchoo,[3,5] L. Gaudefroy,[5] U. Köster,[3] K.-L. Kratz,[2,6] B. Pfeiffer,[2,6] and O. Sorlin[5]

[1]*NSCL, Michigan State University, East Lansing, Michigan 48824, USA*

[2]*Institut für Kernchemie, Universität Mainz, Mainz 55128, Germany*

[3]*ISOLDE, CERN, CH-1211 Geneva 23, Switzerland*

[4]*Departamento de Física Atómica, Molecular y Nuclear, Universidad Complutense, E-28040 Madrid, Spain*

[5]*Institut de Physique Nucleaire d'Orsay, F-91406 Orsay Cedex, France*

[6]*Kernchemie and VISTAR HGF-Virtual Institute for Nuclear Structure and Nuclear Astrophysics, Mainz, Mainz 55128, Germany*

(Received 26 March 2004; published 16 August 2004)

Information on $\beta$-decay properties of neutron-rich $^{47}$Ar was obtained at the ISOLDE facility at CERN using isobaric selectivity. This was achieved by a combination of a plasma-ion source with a cooled transfer line and subsequent mass separation. A doubly charged beam was used in order to improve the signal-to-background ratio associated with multi-charged noble gas fission products. The identification of the $^{47}$Ar $\gamma$-ray transitions was performed by comparing the spectra obtained from direct proton bombardment of the target and of the neutron converter. New excited levels in the daughter $^{47}$K nucleus corresponding to the negative-parity states were observed. The obtained data are compared to the result of large-scale shell model calculations and quasiparticle random-phase approximation predictions.

DOI: 10.1103/PhysRevC.70.024304 PACS number(s): 23.40.−s, 27.40.+z

## I. INTRODUCTION

The nuclear structure of isotopes neighboring doubly magic nuclei is determined to a first approximation by single-particle or hole excitations at presence of an inert core. Thus, information on the structure of these isotopes is especially valuable as it allows simple interpretations and reliable tests of theoretical models. There is surprisingly little known about the $^{47}$K nucleus, which has one proton less than the doubly magic $^{48}$Ca. In early reaction studies [1–3], information on the $1/2^-$ ground state, and the $3/2^+$ first-excited state at 360 keV for $^{47}$K was obtained. In later experiments utilizing the $^{48}$Ca$(d,^3$He$)^{47}$K reaction [4,5] several positive-parity levels corresponding to proton-hole excitations in the *sd* shell were observed up to an excitation energy of 8.5 MeV. In addition, a weakly populated $7/2^-$ state was observed at $\approx$1.97 MeV as reported in Ref. [5]. The assignment of this level was confirmed recently in a brief report [6] on an in-beam spectroscopy experiment using a deep-inelastic heavy ion reaction and the GASP array. The more accurate energy value of the second excited $7/2^-$ state is 2020 keV [6].

Alternatively, information on the structure of $^{47}$K can be obtained from the $\beta$ decay of the $^{47}$Ar nucleus, as selectivity of $\beta$ decay provides information on excited levels that can not be easily populated in nuclear reactions. However, data on the $^{47}$Ar $\beta$ decay is very scarce. Production of the $^{47}$Ar isotope at a fragmentation facility with a $^{48}$Ca primary beam requires the stripping of two neutrons and pickup of one proton. The low cross section of this process only allowed the deduction of the $^{47}$Ar half life in recent experiments performed at GANIL [7,8].

The $^{47}$Ar isotope can also be produced at ISOL facilities. For instance, bombardment of a standard ISOLDE uranium carbide target with a 1–1.4 GeV proton beam from the CERN proton synchrotron booster (PSB) facility provides a sufficient $^{47}$Ar yield. However, some experimental difficulties hinder such a measurement. In general, ionizing noble gas products requires chemically nonselective plasma-ion sources that, for a selected mass, ionize the entire isobaric chain [9]. Using a water-cooled transfer line between target and ion source adds the necessary element selectivity by condensing and depositing all nonvolatile reaction products. Only products gaseous at room temperature are transported via the water-cooled line, ionized in the plasma source and subsequently extracted and mass separated. However, the extracted singly charged extreme asymmetric fission argon products cannot be separated from the doubly charged krypton and triply charged xenon fission products that have the same $A/q$ ratio. Even though the ionization efficiency of the used FEBIAD-type plasma ion source is much lower for ionization to multiply charged ionic states, in-target fission productions in many cases are some orders of magnitude higher than the corresponding values for extreme asymmetric fission products. This results in an overwhelming doubly charged krypton and triply charged xenon background for the singly charged beams of argon isotopes lighter than $^{50}$Ar [10].

The signal-to-background ratio can be improved significantly at the cost of the overall yield by using doubly charged argon beams that correspond to quadruply charged krypton and sextuply charged xenon products. This allowed us to obtain a $^{49}$Ar beam free from the background and deduce information on the gross $\beta$-decay properties of $^{49}$Ar using a $\beta$-neutron detector setup [10]. The doubly charged $^{47}$Ar beam still suffered from a significant multiply-charged fission background, which made measurements with a

*Corresponding author. Email address: weissman@nscl.msu.edu

 

$\beta$-neutron detector setup impossible. On the other hand, use of a triply charged $^{47}$Ar beam would result in a further reduction of the yield by two orders of magnitude [10].

As an alternative, one may consider a measurement performed with a doubly charged beam of $^{47}$Ar, utilizing a $\beta$-$\gamma$-detector setup whenever there is the possibility of identifying the $\gamma$-ray transitions that originate from the different components of the $^{47}Ar^{2+}/^{94}Kr^{4+}/^{141}Xe^{6+}$ mixture. Recently, irradiation of targets by spallation neutrons, produced by bombarding thick metal converters with 1 and 1.4 GeV proton beams, has become common practice at the ISOLDE [12]. The advantage of the use of a neutron converter is the significant reduction of the energy deposited in the targets, and hence, the reduction of the mechanical and thermal stress of the target material. The use of a neutron converter opens an interesting possibility for the identification of the reaction products. In the case of direct bombardment of an actinide target with protons, symmetric and asymmetric fission processes take place. Conversely, extreme asymmetric fission is strongly suppressed in the case of neutron irradiation [13]. Thus, the comparison of the $\gamma$-ray spectra collected for the two cases gives an unambiguous identification of the $\beta$-delayed $\gamma$ rays that originate from the $^{47}$Ar decay.

In this work we present information on the $^{47}$Ar decay obtained by using traditional means to improve the purity of argon beams (a plasma source with cooled transfer line, a mass separation and a doubly charged beam) together with a technique which allowed identification of the $\gamma$ rays of interest in the presence of the complex background.

## II. EXPERIMENT AND RESULTS

### A. Experiment

Neutron-rich argon isotopes were produced in an asymmetric fission reaction induced by a pulsed beam of 1.4 GeV protons ($3\times10^{13}$ protons per pulse) from the PSB accelerator impinging on a standard ISOLDE uranium carbide graphite target. The target contained 44 g/cm$^2$ of $^{238}$U and was heated to about 1900 °C.

The reaction products diffused from the heated target and effused via a low-temperature, water-cooled transfer line to a standard FEBIAD MK-7 plasma ion source [11], where the ionization by plasma discharge took place. The temperature of the transfer line was kept at about 50 °C providing efficient condensation of all elements except noble gases and some other gaseous products. The leakage of nongaseous isobars through the cooled line was found to be negligible. A tungsten converter (12.7 mm diameter, 125 mm length) was placed parallel to the target at a distance of 22 mm axis to axis [12], that allowed one to switch to the neutron irradiation of the target by changing the focus of the proton beam from the target to the converter. The implantation point was surrounded by four 125 $\mu$m Kapton windows transparent to high-energy $\beta$ particles. Four 1.5-mm-thick plastic detectors were positioned close to the Kapton windows for detecting $\beta$ particles. The detailed description of the $\beta$ detectors is given in Ref. [10]. Two Ge detectors of 75% and 65% relative efficiency were placed next to the implantation point for detecting $\gamma$ rays. The time and energy signals were collected by a VME-based data acquisition system. The trigger included only the time signals from the four $\beta$ detectors. The time window for acquisition was 26 $\mu$s. The detection times of the $\gamma$ rays and $\beta$ particles were recorded by a precise time-stamping module. Each registered event consisted of the time relative to the proton beam hitting the target, and a pattern word to indicate the detectors that were triggered in the event.

The efficiencies of the $\beta$ and $\gamma$ detectors were measured using $^{45,46}$Ar, $^{23-26}$Ne, $^{90}$Kr sources collected on line, corresponding to a broad energy range of emitted $\gamma$ rays. The detection efficiency for $\beta$ particles was measured by comparing singles and $\beta$-gated Ge spectra and was found to be 35(4)%. The on-line calibration sources had to a first order the same geometry as the investigated $^{47}$Ar source. The intensity of the on-line sources was kept low to avoid dead-time effects. Decay curves gated by $^{25,26}$Ne and $^{94}$Kr $\gamma$-ray transitions yielded half lives of the corresponding nuclei and were used to cross-check the performance of the time-stamp module. The coincidences between a Ge detector and the adjacent $\beta$ detector allowed one to veto of a $\beta$ particle signal in the Ge energy spectra.

Special efforts were made to minimize the effects of $^{47}$Ar diffusion from the surface of the aluminized tape after implantation. A new aluminized Mylar tape was installed before the experiment. In our previous work [14] small diffusion was observed even for implantation into an aluminum host. The analysis of the time profiles [14] showed that the effects of diffusion on the obtained half lives are negligible if the time of implantation, determined by the duration of the beam gate period (the time window after a proton pulse for the extracted beam to be transported through the separator), is larger than the time of diffusion ($\approx$50 ms for singly charged argon implanted at 60 keV). Thus the use of much longer implantation time ensures that the diffusion effect can be neglected.

### B. Results

Two examples of $\gamma$-ray spectra collected for an $A/q$ value of 23.5 for direct proton bombardment of the target and of the neutron converter are shown in Fig. 1. Both spectra were taken for the same time cycle corresponding to a proton pulse repetition of 2.4 s. The beam gate was open for 700 ms after each pulse, after a short 40 ms delay. The tape was moved 2 s after every proton pulse to remove the long-lived decay products before the next implantation. The lower statistics in the neutron-converter spectrum correspond to the shorter collection time and the generally lower yield due to the geometrical efficiency factor [12].

A rich variety of $\gamma$-ray transitions belonging to the decay cascades of the $^{47}$Ar/$^{94}$Kr/$^{141}$Xe implanted nuclei is observed in the spectra. One can also observe the striking difference between the two spectra due to some peaks, which are not seen in the neutron-converter spectrum. The latter are 360, 1660, 1742, 2020, 3207, 3402, 3718, and 3822 keV $\gamma$-ray transitions. These transitions are possible members of the $^{47}$Ar decay cascade. Some weaker high-energy transitions, 3316, 3357 and 4010 keV, are also observed for the

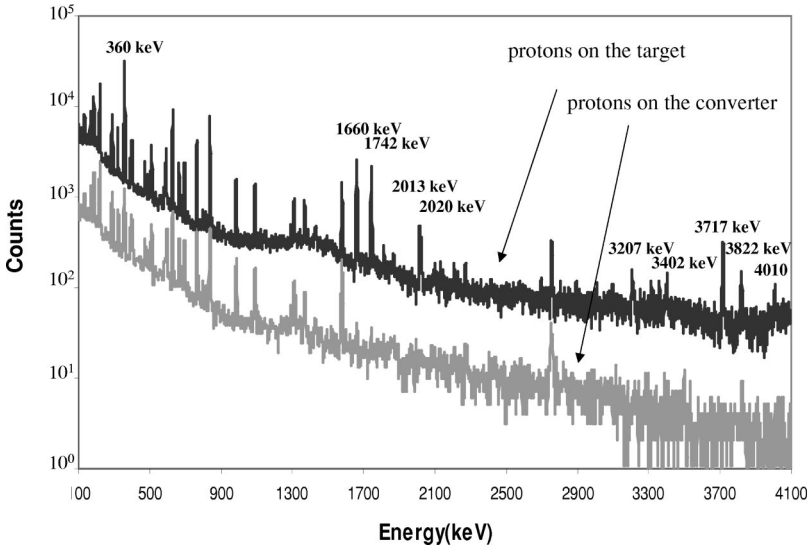


FIG. 1. Examples of $\beta$-gated $\gamma$-ray spectra collected for the $A/q=23.5$ separator setting for direct proton bombardment of the target and for the neutron conversion. The energy of the transitions that are enhanced in the former spectrum are indicated.

case of direct bombardment. A contamination to the 360 keV transition seen in the neutron-converter spectrum corresponds to the $^{94}$Kr and $^{141}$Xe $\gamma$ rays (359 keV and 362 keV). The 2013 keV transition of $^{47}$K is strongly suppressed in the direct-bombardment spectrum due to the tape movement. The relative intensities of the transitions of interest, corrected for the detector efficiencies, are summarized in Table I. The background to the 360 keV transition was subtracted using the spectrum obtained with the neutron converter. The application of gates on the strongest $\gamma$-ray transitions indicates correlations between the 360, 1660, 1742 and 3822 keV lines (Fig. 2 and Table I). A 629 keV transition observed in coincidence with the 360 keV line (Fig. 2) is due to an incomplete subtraction of a $^{94}$Kr background line. No coincidences were found with the relatively strong 3718 keV transition. The obtained statistics do not allow one to observe any coincidences in the spectra gated by the weaker transitions.

The time decay curves gated by the $\gamma$ transitions of interest are shown in Fig. 3. The background, obtained by applying the same gates on the data taken with the neutron converter, was subtracted. The transitions of interest exhibit similar half lives of the order of 1.2 s, confirming the assumption that they originate from the same decay. In addition to the data presented in Fig. 3, another set of data with different beam cycle settings, allowing the longer decay time (pulse each 3.6 s, beam gate was open for 1 s after each pulse following a 30 ms delay and tape was moved in 3.2 s after each pulse) was used to obtain the half lives. A summary of the obtained half lives is presented in Table I.

A separate measurement was performed to obtain information on the neutron emission probability, $P_n$, in the $^{47}$Ar decay. The tape was not moved, allowing one to measure the intensity of the longer-lived $^{47}$K and $^{46}$K decay products. The measuring time was approximately 1 h, much longer than the half lives of the $^{47}$K and $^{46}$K nuclei. None of the $^{46}$K transitions, including the strongest 1368 keV transition, was observed, which corresponds to a small neutron emission probability. The obtained upper limit for the $P_n$ value is 0.2%. The relative intensities of the 586 and 2013 keV transitions, belonging to the $^{47}$K decay, were obtained in the same measurement (Table I).

TABLE I. The relative intensities, half lives and cascade partners of the $^{47}$Ar $\gamma$ rays. The relative intensities of the 586 and 2013 keV transitions from $^{47}$K decay obtained in the experiment without tape movement are also shown.

| Energy (keV) | Rel. int. | Half life (ms) | Coincidences |
|---|---|---|---|
| 360 | 100 | 1230(35) | 1660, 1742, 3822 |
| 1660 | 53(5) | 1240(70) | 360, 1742, 3822 |
| 1742 | 41(4) | 1350(117) | 360, 1660 |
| 2020 | 7(1) | 1220(160) | |
| 3207 | 3(1) | | |
| 3316 | 1(1) | | |
| 3357 | 1(1) | | |
| 3402 | 4(2) | | |
| 3718 | 14(2) | 810(290) | |
| 3822 | 6(1) | $\leqslant$1300 | 360, 1660 |
| 4010 | 3(1) | | |
| 586 | 147(16) | | |
| 2013 | 155(15) | | |

## III. DISCUSSION

The $\gamma$-ray transitions, observed only in the direct target bombardment spectra, originate from an asymmetric fission product, the transitions exhibit the similar half life. These facts, together with the chemical selectivity of a plasma ion source with the cooled transfer line, suggest that the transitions of interest belong to the $\beta$ decay of $^{47}$Ar.

A tentative $^{47}$Ar decay scheme is presented in the left plate of Fig. 4 and Table II. The position of the first two excited levels and the corresponding 360 and 1660 keV transitions in $^{47}$K are known from Ref. [6]. The 1742 and 3822 keV transitions are placed according to the observed coincidence relations. The relatively strong 3718 keV transition is not in coincidence with any other $\gamma$-ray line. Therefore it is assumed to be emitted from a 3718 keV excited level directly to the ground state. A tentative placement of

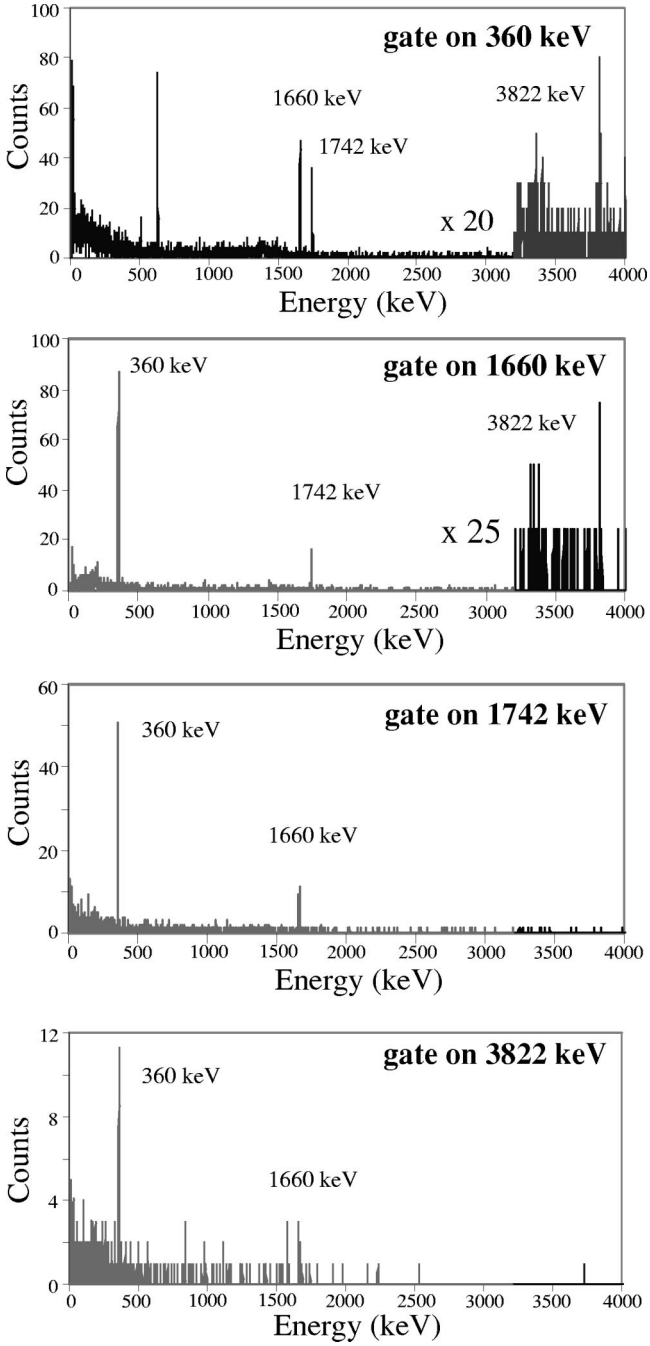


FIG. 2. The $\gamma$-ray spectra gated by some of the transitions of interest.

some weak transitions (2020, 3402, 3357 keV) was done only due to their energy values. Some of the observed high-energy transitions (3207, 3316 and 4010 keV) were not placed in the scheme.

As a leakage of the $^{47}$K isobar through the cooled transfer line of the plasma source was negligible, the observed $^{47}$K activity corresponds to the buildup of the $^{47}$Ar daughter product. Thus, the intensities of the 2013 and 586 keV $^{47}$K transitions (Table I) represent the 93% and 79% parts of the total $^{47}$Ar decay flux, respectively [15]. The total strength of $^{47}$Ar decay measured in these transitions is 174(13) in the relative intensity units of Table I. This value should be compared with the sum of intensities of the 360, 2020, 3718, 3207, 3316, and 4010 keV $\gamma$ rays populating the $^{47}$K ground state, 128(3). One can assume that the undetected decay to the ground state is responsible for the rest of the decay strength, 46(13) units, that corresponds to a 26(8)% decay branching to the ground state.

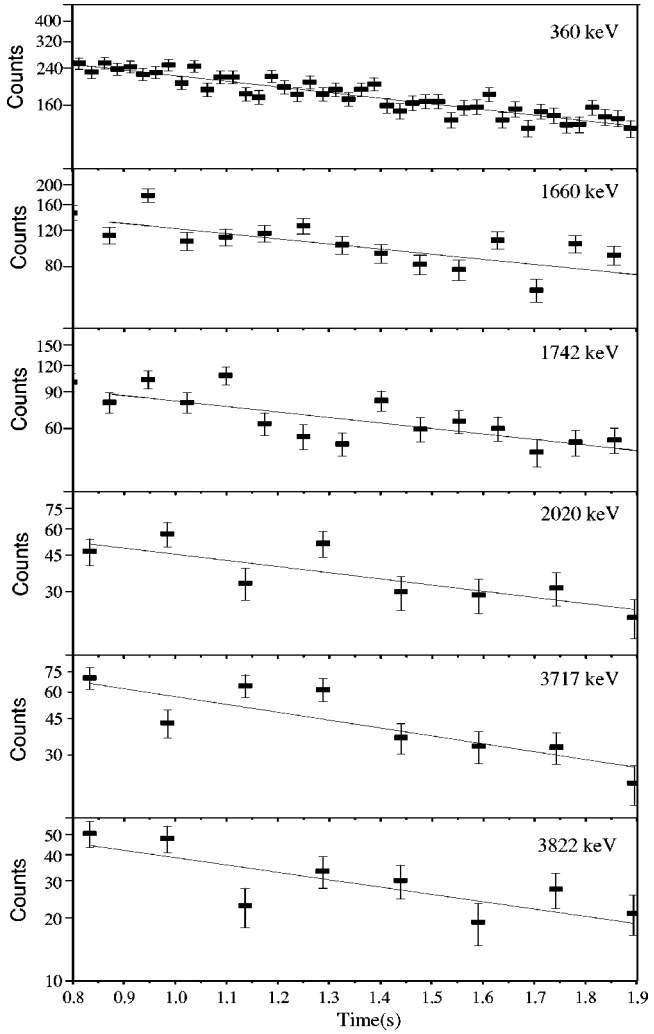


FIG. 3. The results of fitting the decay curves gated by the $\gamma$-ray transitions of interest.

The deduced properties of $^{47}$Ar decay are summarized in Table II and Fig. 4. The branching ratios are normalized by the total decay flux. The decays to the ground state, the 360 and 2020 keV levels, were assumed to be first forbidden and their $\log f_1 t$ values were calculated in accordance with Ref. [16]. The adopted $^{47}$Ar half life is 1.23(3) s, in good agreement with the value reported in Ref. [8] [1.25(15) s].

Shell-model calculations were carried out with the code OXBASH [18] in the *sd-pf* model space with truncations built around the closed-shell structure of $(sd)^{24}(f_{7/2})^8$ for $^{48}$Ca. In analogy with other known $N=29$ isotones, $^{47}$Ar is expected to have a ground-state spin and parity of $3/2^-$. For $^{47}$Ar we assume the negative parity $(3/2^-)$ ground state to be two-hole one-particle configurations $(sd)^{22}(f_{7/2})^8(f_{5/2},p_{3/2},p_{1/2})$. For $^{47}$K, we take for positive-parity states $(sd)^{23}(f_{7/2})^8$ and $(sd)^{23}(f_{7/2})^7(f_{5/2},p_{3/2},p_{1/2})$, and

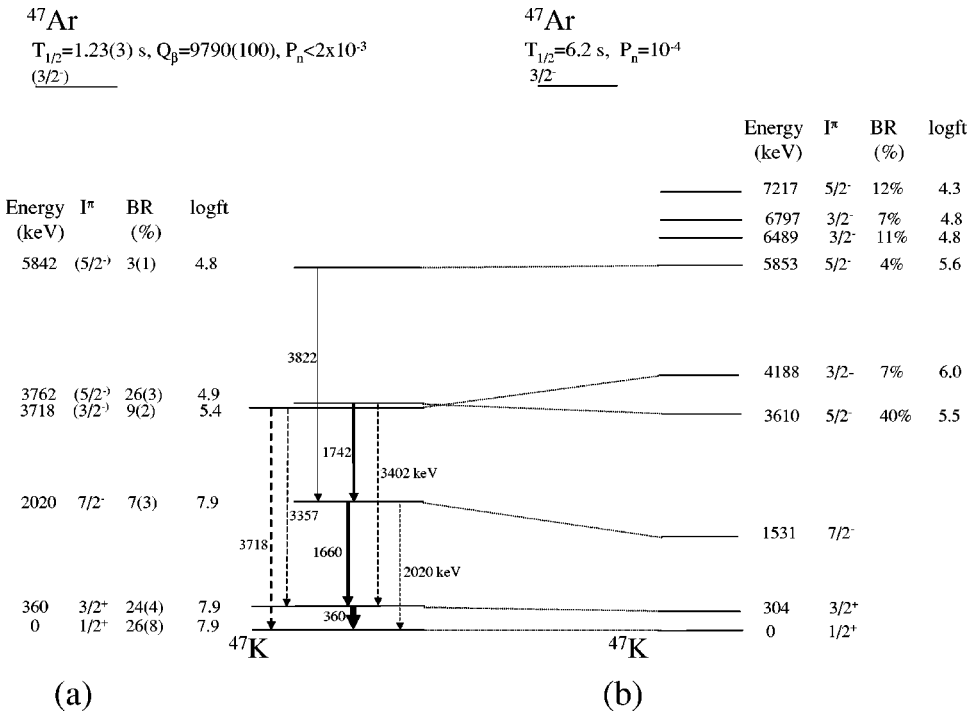


FIG. 4. Tentative scheme of $^{47}$Ar decay compared with the results of the shell-model calculations. The decay $Q_\beta$-value is taken from Ref. [17].

for negative-parity states $(sd)^{22}(f_{7/2})^8(f_{5/2},p_{3/2},p_{1/2})$ and $(sd)^{22}(f_{7/2})^9$. The occupation of the various configurations that contribute to the negative parity states are presented in Table III. Only configurations with contributions larger than 10% are listed. The negative-parity states are formed by combinations of different configurations corresponding to promoting protons from the *sd* shell across the gap. The first $5/2^-$ state has according to the calculation a main component (56%) from coupling the angular momenta of $d_{3/2}$, $s_{1/2}$ and $f_{7/2}$ protons. Except for this component, the state is fragmented with all components contributing less that 10% to the overall wave function. Also, according to the calculation, the $3/2^-$ state is fragmented into four major configurations. The main one of these arises when the odd protons in the $d_{3/2}$ and $s_{1/2}$ orbitals now couple to a proton in the $f_{7/2}$ orbital. The second $5/2^-$ state contains again two of the configurations similar to the ones in the $7/2^-$ state but with excitations in the *sd* shell.

TABLE II. Tentative level assignment, energies, branching ratios, and logft values of the $^{47}$K levels. The decays to the ground state and to the 360 and 2020 keV levels were assumed to be first forbidden and their $\log f_1 t$ were calculated according to Ref. [16]. All branching ratios are normalized on the total decay strength deduced from intensities of the $^{47}$K transitions.

| $I^\pi$ | $E$ (keV) | $I_\beta$ (%) | Logft |
|---|---|---|---|
| $1/2^+$ | 0 | 26(8) | 7.9 |
| $3/2^+$ | 360 | 24(4) | 7.9 |
| $7/2^-$ | 2020 | 7(3) | 7.9 |
| $3/2^-$ | 3718 | 9(2) | 5.4 |
| $5/2^-$ | 3762 | 26(3) | 4.9 |
| $5/2^-$ | 5842 | 3(1) | 4.8 |

The lowest energy states in $^{47}$K are positive parity and can be reached from $^{47}$Ar decay by first-forbidden transitions. The negative-parity states, which start with the $7/2^-$ at 1.53 MeV, can be reached by allowed (Gamow–Teller) decay. This is the only decay we are able to calculate.

The two-body Hamiltonian was taken from Ref. [19]. The single-particle energies were adjusted to approximately reproduce the single-particle spectra of $^{48}$Ca ($f_{7/2}$), $^{49}$Ca ($p_{3/2},p_{1/2}$, and $f_{5/2}$) and $^{47}$K ($s_{1/2},d_{3/2}$ and $d_{5/2}$). Thus the theoretical spectrum for $^{47}$K shown in the right plate of Fig. 4 is adjusted to reproduce the $1/2^+$ and $3/2^+$ energies, but the energies of the higher states are predicted by calculations as well as with the allowed decay to the negative parity ex-

TABLE III. Theoretical compositions of the negative-parity levels. Only configurations contributing more than 10% are presented.

| Level | Configuration | Occupation |
|---|---|---|
| $7/2^-$ | $(d_{5/2})^{12}(d_{3/2})^8(s_{1/2})^2(f_{7/2})^9$ | 35% |
| | $(d_{5/2})^{12}(d_{3/2})^6(s_{1/2})^4(f_{7/2})^9$ | 32% |
| | $(d_{5/2})^{12}(d_{3/2})^7(s_{1/2})^3(f_{7/2})^8(p_{3/2})^1$ | 10% |
| $3/2^-$ | $(d_{5/2})^{12}(d_{3/2})^7(s_{1/2})^3(f_{7/2})^9$ | 37% |
| | $(d_{5/2})^{12}(d_{3/2})^6(s_{1/2})^4(f_{7/2})^8(p_{3/2})^1$ | 17% |
| | $(d_{5/2})^{12}(d_{3/2})^6(s_{1/2})^4(f_{7/2})^9$ | 15% |
| | $(d_{5/2})^{12}(d_{3/2})^8(s_{1/2})^2(f_{7/2})^8(p_{3/2})^1$ | 13% |
| $5/2^-_1$ | $(d_{5/2})^{12}(d_{3/2})^7(s_{1/2})^3(f_{7/2})^9$ | 56% |
| $5/2^-_2$ | $(d_{5/2})^{12}(d_{3/2})^6(s_{1/2})^4(f_{7/2})^9$ | 38% |
| | $(d_{5/2})^{12}(d_{3/2})^7(s_{1/2})^3(f_{7/2})^9$ | 33% |

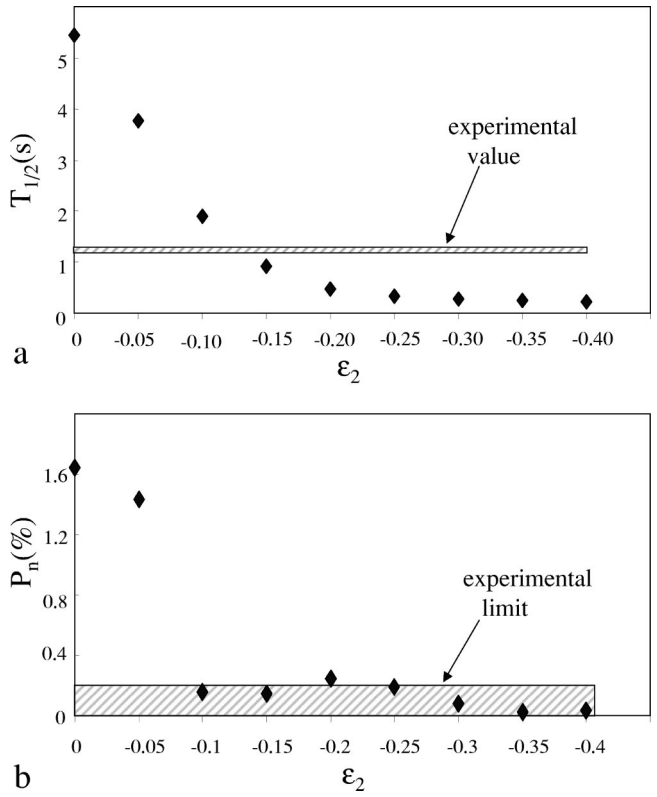


FIG. 5. The results of the enhanced QRPA calculations of the gross $\beta$-decay parameters are compared with the experiment.

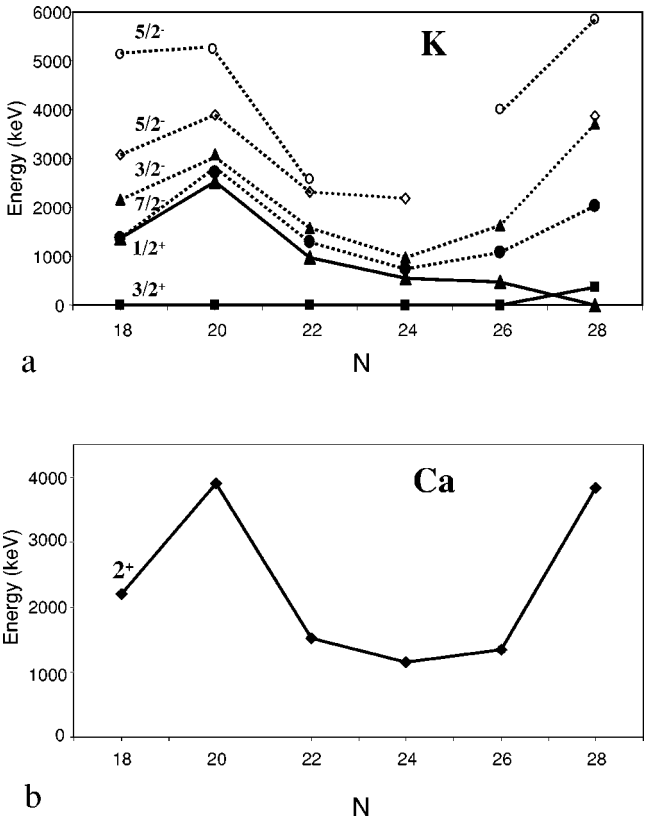


FIG. 6. (a) Systematics of level energies in the odd potassium isotopes. (b) Systematics of energies of $2^+$ levels in the corresponding even calcium isotopes.

cited states. The Gamow–Teller decay was calculated with the free-nucleon value $|g_A/g_V|=1.26$.

The calculated half life is significantly longer than the measured one. Calculated half lives are often shorter than those measured, and this is interpreted in terms of an effective quenching of the $|g_A/g_V|$ value [20]. The present experiment shows that first-forbidden decay branches to the first-excited level and ground state are 24% and 26%, respectively. Thus, the strong contribution of the forbidden decays to the ground and the first excited states may be responsible for the discrepancy between the experiment and the calculated half life which is a partial lifetime for the allowed decay.

The results of the calculations are very useful for understanding the decay scheme. The spin parity of the 2020, 3718, 3762, and 5842 keV levels can be tentatively assigned as $7/2^-$, $3/2^-$, $5/2^-$ and $5/2^-$, respectively, by comparison of the experimental and the calculated decay patterns. The calculated ground state of $^{47}$Ar corresponds to the $3/2^-$ state, the experimental branching ratios to the $7/2^-$, $3/2^-$ and $5/2^-$ levels of $^{47}$K are consistent with this assignment. The calculated $P_n$ value is in good agreement with the obtained experimental upper limit. The results of the calculations suggest that a significant part of the decay proceeds via feeding of the highly excited states. It is possible that the high-energy transitions (3207, 3316, and 4010 keV) that were not placed in the tentative scheme correspond to the decay from these highly excited levels.

The $\beta$-decay half life, $T_{1/2}$, and $\beta$-delayed neutron-emission probability, $P_n$, were also calculated using a microscopic quasiparticle random-phase approximation (QRPA) [21]. The Folded–Yukawa potential and Lipkin–Nogami pairing interaction were used in the model. Recently this standard QRPA model has been enhanced to account for first-forbidden decays [22], the latter were calculated in the statistical gross theory [23]. The typical contribution of the first-forbidden decays in the $\beta$-strength function is of the order of 10–15%. As the gross $\beta$-decay properties ($T_{1/2}$ and $P_n$) are very sensitive to the nuclear deformation, the comparison of the experiment and calculations for an assumed nuclear shape may give some useful insight into the nuclear structure. The QRPA calculations [24] predict two possible minima, nearly spherical, $\epsilon_2=0.033$, and slightly oblate, $\epsilon_2=-0.183$. We have performed the QRPA calculations for different values of oblate deformation with $\epsilon_2$ ranging from 0 to $-0.4$. The results of the calculated $T_{1/2}$ and $P_n$ are shown in Figs. 5(a) and 5(b). One can observe from Figs. 5(a) and 5(b) that the experimental result favors the slightly oblate nuclear shape, $-0.1>\epsilon_2>-0.15$.

Considerable interest in the nuclear structure around $^{48}$Ca is driven by the recent discovery of rapid weakening of the $N=28$ shell in the sulfur and chlorine isotopes [7,25,26]. It is interesting to examine if the $N=28$ shell closure persists for the corresponding argon and potassium isotopes. The $B(E2)$ value of the first excited level in $^{46}$Ar obtained via Coulomb excitation demonstrated that the spherical gap stays intact for this nucleus [25]. Comparison of half life and $P_n$ values of the heavier $^{49,50}$Ar isotopes with the enhanced QRPA calcu-

lations [10] indicates that these nuclei have only slight oblate deformation. The same conclusion is reached in the present work regarding the $^{47}$Ar nucleus.

The information on the $^{47}$K levels allows the extension of the systematics of the level energies as a function of the number of neutrons in the $f_{7/2}$ shell [Fig. 6(a)]. Some of the highly excited $5/2^-$ levels in $^{43,45}$K are not known unambiguously and were omitted from Fig. 6. However, the general trend is clear: the energies of the $5/2^-$, $3/2^-$ and $7/2^-$ levels decrease after passing the $N=20$ magic number and increase again towards the next $N=28$ closed neutron shell. The behavior of the $1/2^+$ level is rather different. The energy gap between the $s_{1/2}$ state and the $d_{3/2}$ ground state is 2522 keV at $N=20$ and gradually decreases down to $-360$ keV for $N=28$, corresponding to the $1/2^+$ ground state. Such behavior of the $1/2^+$ state is due to the difference between its and higher $l$ states interaction strengths with the $\nu f_{7/2}$ neutron orbit being filled with neutrons. This phenomenon was discussed in [27,28] and more recently in [29] and should not be confused with weakening of the shell closure. The energies of the levels in the neutron-rich potassium isotopes exhibit typical shell closure features [Fig. 6(a)] that can be compared with systematics of the $2^+$ levels in the corresponding calcium isotopes [Fig. 6(b)]. This, and all arguments above, suggest that the $N=28$ shell weakening observed in lighter nuclei does not take place for the argon and potassium chains.

## IV. CONCLUSION

Information on the $^{47}$Ar decay was obtained using a plasma ion source with a cooled transfer line and mass separation. The purity of the beam was improved by using a doubly charged beam. A technique, comparing the $\gamma$-ray spectra obtained by direct bombardment of the target and of the neutron converter, allowed the identification of the $^{47}$Ar $\gamma$ rays in the presence of a complex background. Negative-parity levels of $^{47}$K were observed, and the $^{47}$Ar half life, the upper limit for neutron emission probability and decay branching ratios, was deduced. The tentatively proposed decay scheme is in agreement with the results of large scale shell-model calculations. The experimental and theoretical results suggest that the ground state of $^{47}$Ar is $3/2^-$. The results of the QRPA calculations favor a moderately oblate shape of the $^{47}$Ar nucleus. The obtained data confirm that the $N=28$ shell closure persists for the argon and potassium isotopic chains.

## ACKNOWLEDGMENTS

We would like to thank the ISOLDE collaboration for support of this experiment and the crew of the PSB-ISOLDE facility for operation of the separator and the ion source. We would like to acknowledge financial support by the European Commission Contract Nos. HPRI-CT-1999-00018 and HPRI-CT-2001-50033.

[1] D. C. Williams, J. D. Knight, and W. T. Leland, Phys. Lett. **22**, 162 (1966).
[2] J. H. Bjerregaard, O. Hansen, O. Nathan, R. Stock, R. Chapman, and S. Hinds, Phys. Lett. **24B**, 568 (1967).
[3] R. Santo, R. Stock, J. H. Bjerregaard, O. Hansen, O. Nathan, R. Chapman, and S. Hinds, Nucl. Phys. **A118**, 409 (1968).
[4] P. Doll, G. J. Wagner, K. T. Knöpfle, and G. Mairle, Nucl. Phys. **A263**, 210 (1976).
[5] S. M. Banks *et al.*, Nucl. Phys. **A437**, 381 (1985).
[6] R. Broda, Acta Phys. Pol. B **32**, 2577 (2001).
[7] O. Sorlin *et al.*, Nucl. Phys. **A583**, 763 (1995).
[8] S. Grevy *et al.*, Nucl. Phys. **A722**, 424 (2003).
[9] M. V. Ricciardi *et al.*, Nucl. Phys. **A701**, 156c (2002).
[10] L. Weissman *et al.*, Phys. Rev. C **67**, 054314 (2003).
[11] T. Bjørnstad *et al.*, Phys. Scr. **34**, 578 (1986).
[12] R. Catherall, J. Lettry, S. Gilardoni, and U. Köster, Nucl. Instrum. Methods Phys. Res. B **204**, 235 (2003).
[13] A. C. Wahl, At. Data Nucl. Data Tables **39**, 1 (1988).
[14] U. C. Bergman *et al.*, Nucl. Phys. **A714**, 21 (2003).
[15] R. B. Firestone, *Table of Isotopes* (Wiley, New York, 1996).
[16] N. B. Gove and M. J. Martin, Nucl. Data Tables **10**, 205 (1971).
[17] G. Audi, A. H. Wapstra, and C. Thibault, Nucl. Phys. **A729**, 337 (2003).
[18] A. Brown, A. Etchegoyen, and W. D. M. Rae, computer code OXBASH, MSU-NSCL, Report No. 524.
[19] E. K. Warburton, J. A. Becker, and B. A. Brown, Phys. Rev. C **41**, 1147 (1990).
[20] B. A. Brown and B. H. Wildenthal, At. Data Nucl. Data Tables **33**, 347 (1985).
[21] P. Möller, J. R. Nix, and K.-L. Kratz, At. Data Nucl. Data Tables **66**, 131 (1997).
[22] P. Möller, B. Pfeiffer, and K.-L. Kratz, Phys. Rev. C **67**, 055802 (2003).
[23] K. Takahashi, M. Yamada, and T. Kondoh, At. Data Nucl. Data Tables **12**, 101 (1973).
[24] P. Möller (private communications).
[25] H. Scheit *et al.*, Phys. Rev. Lett. **77**, 3967 (1996).
[26] T. Glasmacher *et al.*, Phys. Lett. B **395**, 163 (1997).
[27] R. K. Bansal and J. B. French, Phys. Lett. **11**, 145 (1964).
[28] P. Martin, N. Buenerd, Y. Dupont, and M. Chabre, Nucl. Phys. **A185**, 465 (1972).
[29] P. D. Cottle and K. W. Kemper, Phys. Rev. C **58**, 3761 (1998).